Porous silicon micro-resonator implemented by standard photolithography process for sensing application

Pauline Girault, Paul Azuelos, Nathalie Lorrain, Luiz Poffo, Jonathan Lemaitre, Parastesh Pirasteh, Isabelle Hardy, Monique Thual, Mohammed Guendouz, Joël Charrier

Porous silicon micro-resonator implemented by standard photolithography process for sensing application

P. Girault[1*], P. Azuelos[1], N. Lorrain[1], L. Poffo[1], J. Lemaitre[1], P. Pirasteh[1], I. Hardy[1,2], M.Thual[1], M. Guendouz[1] and J. Charrier[1]

[1]UMR FOTON, CNRS, Université de Rennes 1, Enssat, F22305, Lannion, France

[2]UMR FOTON, CNRS, IMT Atlantique, F29238, Brest, France

* Corresponding author: pgirault@enssat.fr

Abstract

A micro-resonator based on porous silicon ridge waveguides is implemented by a large scale standard photolithography process to obtain a low cost and sensitive sensor based on volume detection principle instead of the evanescent one usually used. The porous nature of the ridge waveguides allows the target molecules to be infiltrated in the core and to be detected by direct interaction with the propagated light. Racetrack resonator with radius of 100 µm and a coupling length of 70 µm is optically characterized for the volume detection of different concentrations of glucose. A high sensitivity of 560 nm/RIU is reached with only one micro-resonator and a limit of detection of 8.10^{-5} RIU, equivalent to a glucose concentration of 0.7 g/L, is obtained.

Keywords: Sensors; Integrated optics; Optical design and fabrication; Resonators; Porous silicon

1. Introduction

The ability to rapidly detect, identify and monitor chemical or biological species is critical in many economic and societal problems such as environmental monitoring, health monitoring and security applications. The detection of bio-chemicals traces requires analytical tools which can detect these traces within an acceptable time, sensitive enough to detect really low concentrations and selective not to be affected by other factors in the environment. It is now well-established that the development of compact portable sensors and analyzers can be of great help to overcome the inherent limitations of laboratory techniques in terms of both spatial and temporal resolutions.

Micro Resonators (MRs) are now widely investigated for sensing applications. High quality factors up to 10^8 can be obtained with microspheres [1, 2] which allow to achieve low optical detection limits as they are able to react to a monolayer of molecules adsorption [3, 4, 5]. However, microsphere resonators lack of integration capability [6], which limits their use in practical applications in integrated optics. To solve these problems, integrated micro-ring, racetrack or micro-disk resonators are used, albeit with reduced Q factors [7] in the range of 10^4-10^5. They can be integrated on Photonic Integrated Circuits (PIC) which provide a route toward small, low-cost and very rugged optical systems and could therefore be a game-changer for sensor systems. Most integrated sensors developed up to now are geared toward classical surface detection by using evanescent wave sensing: the most studied materials used for sensing applications are bulk semiconductors or polymers and the detection principle is based on interaction of the probed molecules with the evanescent part of a wave [7]. This interaction leads to a wavelength shift of the MR response depending on the refractive index variation induced by

the probed molecules. The sensitivity is thus defined as the ratio between this wavelength shift and the refractive index variation in nm/RIU (Refractive Index Unit). Sensitivities of 200 nm/RIU and of 230 nm/RIU have been obtained respectively using bulk material with one polymer micro-ring for glucose detection [8] or with one Si_3N_4 micro-disk for LiCl detection [9].

However, the sensitivity of integrated MRs can be improved by optimizing the interaction between the molecules and the optical wave. This optimization can be provided by the use of a porous material such as porous silicon (PS) for the waveguide core. In this case, the principle of the sensor is based on a volumic detection which allows a direct interaction between the propagated light and the molecules to be detected [10, 11,12].

Indeed PS is a widely studied material regarding its optical properties in many applications in optoelectronics [13] and also over the past decade for chemical [14,15] and biological sensing [16, 17]. The large internal surface of porous silicon and its biocompatibility constitute significant advantages for biosensing [18]. This material is used as a host to various molecules that can be in solution in the pores, or grafted to the internal surface of silicon after its functionalization [17]. Optical PS sensors using refractive index variation have already been the subject of various studies [11,12], the number of which continues to grow due to the interest of this porous material to increase the sensitivity of the sensors. Recently the first all porous single side coupled micro-ring resonators obtained with e-beam lithography, allowed to reach a detection sensitivity of 380 nm/RIU when salt water solutions are infiltrated into the device [19].

In this paper, the work aims to study an all porous single side coupled micro-racetrack resonator fabricated with a large scale standard photolithography process and to enhance the sensitivity of the sensor. In a first part, the design, the fabrication and the setup of optical characterization around 1550 nm are described. On the second part, the results of optical

characterization of the MR are reported and homogeneous sensing experiments using glucose aqueous solution with high sensitivity are presented.

2. Experimental

2.1. Materials and design

Three consecutives PS layers have been prepared by electrochemical anodization of a heavily doped P (100) silicon substrate with a 5 mΩ.cm resistivity and using applied current densities of respectively 1, 50 and 80 mA/cm^2 for specific times. The electrolyte was formed by combining hydrofluoric acid (50 %) with ethanol and deionized water in the ratio of 2-2-1 respectively. Following this, the PS layers were partially oxidized at 500°C for 5 min to passivate the surface and to obtain a hydrophilic surface.

The first PS layer (1 mA/cm²) is a thin barrier layer with a very low porosity on the top of the two other layers constituting the core and the cladding layers of the PS waveguide. The current densities of these two layers have been chosen both to get high porosities after oxidation treatment to reach high MR sensor sensitivity and to get a single mode propagation with micronic dimension waveguides. This structure with three layers will be submitted to a photolithographic process inducing a photosensitive resin deposit, thus the first layer constitutes a barrier layer that will prevent the infiltration of this resin in the two lower layers.

The thickness of each porous layer has been fixed and then verified by cross section SEM (Scanning Electron Microscope) measurements. From these thicknesses, porosities and then refractive indices are determined by the adjustment of the calculated reflectance spectra of each porous layer with the experimental ones using Bruggemann model [20, 21]. The partial oxidation

step of porous layers induces a porosity decreasing due to silica expansion [22]. The values of porosities and refractive indices of the PS layers (core and cladding), are given in Table I. Values of refractive indices for the porous layers are given initially with air superstrate ($n_{air\ superstrate}$) and have also been calculated with a deionized water superstrate ($n_{water\ superstrate}$) as the MR will be used for sensing experiment with glucose solubilized in deionized water. The water infiltrates pores, that is why the refractive index of each layer increases. The characteristics of the first layer are not indicated as it is a barrier and a sacrificial layer that will be removed thereafter during the process.

Table I: Thickness, porosity and refractive index (@1550 nm) for air and deionized water superstrate for the partially oxidized PS layers.

Porous layers	Thickness (µm)	Porosity before oxidation (%)	Porosity after partial oxidation (%)	$n_{air\ superstrate}$ (after oxidation)	$n_{water\ superstrate}$ (after oxidation)
Core	2.0 ± 0.1	66 ± 2	56 ± 2	1.55 ± 0.06	1.77 ± 0.06
Cladding	5.0 ± 0.1	73 ± 2	63 ± 2	1.38 ± 0.06	1.62 ± 0.06

2.2. Fabrication: straight ridge waveguide and micro-resonator

PS ridge waveguides have been implemented using a large scale standard photolithography process on the PS layers. The process is described for the PS MR in Fig. 1.a, 1.b and 1.c. A positive SPR photosensitive resin layer is deposited by spin coating on the top of the structure, constituted by the thin barrier. Patterns are then produced under UV exposure through a well-defined chrome mask designed using commercial Olympios software. To obtain the aimed PS ridge waveguides, a first trifluoromethane (CHF_3) RIE (Reactive Ion Etching) - ICP (Inductively Coupled Plasma) plasma is performed to remove both the barrier and core layers unprotected by

the resin (Fig. 1.b). Once the cladding layer is reached, a O_2 RIE - ICP plasma is applied to etch the residual resin. Finally, the barrier layer is removed from the obtained waveguides by a CHF_3 RIE - ICP plasma.

The aimed dimensions of the PS ridge waveguides are a height of 2 µm and a width of 2 µm in order to obtain a single mode propagation. A previous study on porous silica MR has led to the design of MR with several radius, coupling length and gap values [23]. Among the different studied MR geometries, a racetrack PS MR with a radius R of 100 µm and a coupling length Lc of 70 µm has been chosen (Fig. 1.d). The straight and the racetrack MR ridge waveguides are separated by a gap of 0.5 µm. These values have been chosen because they allow to obtain the coupling ratio near the critical one which enables optimal contrast of the transfer function with a deionized water superstrate.

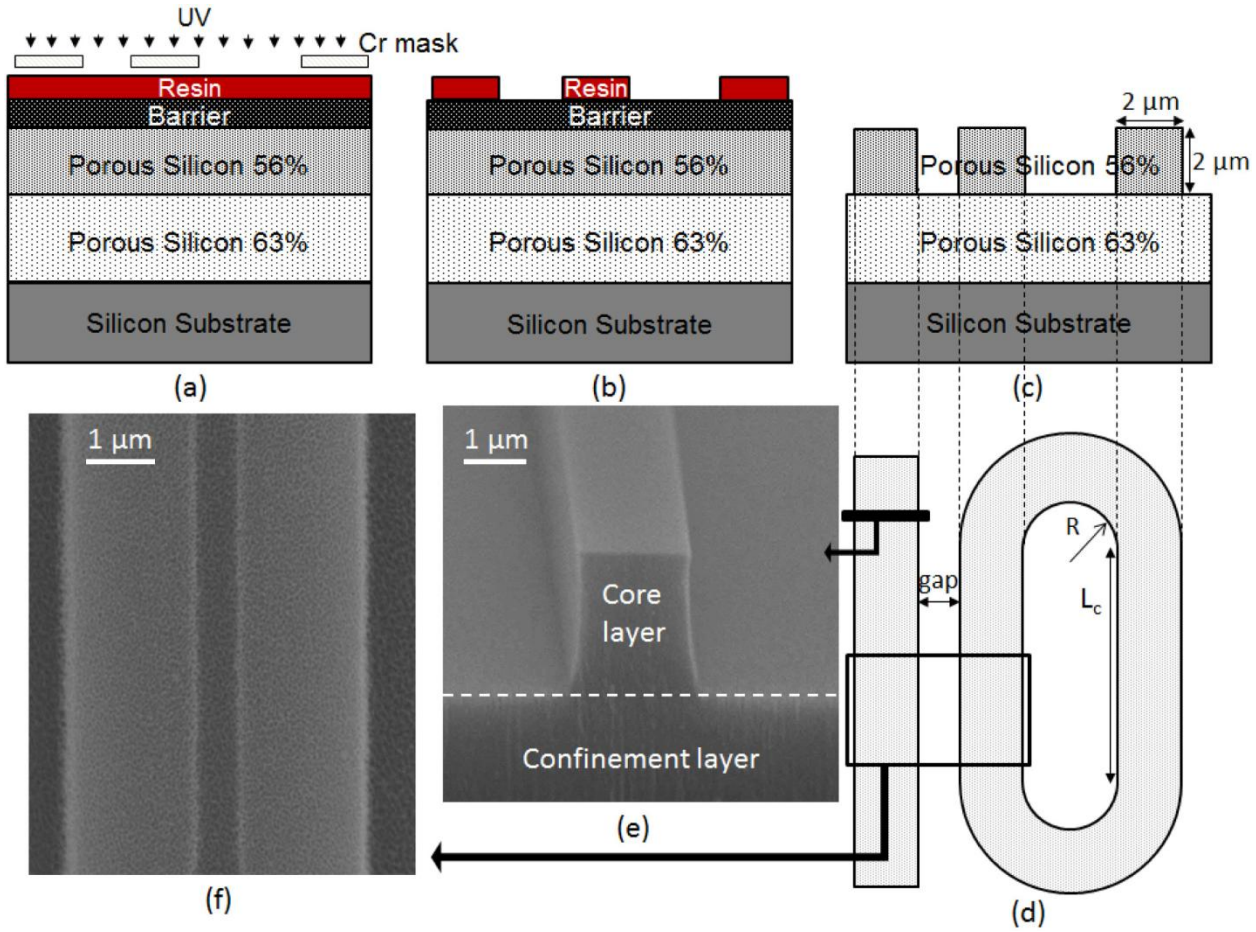

Fig. 1. Schema of the photolithography process used for the fabrication of PS ridge waveguides: a) deposit of a SPR photosensitive resin and irradiation under UV exposure; b) wet etching development of the photosensitive resin; c) dry etching of the PS layers ("barrier" and core) under the unprotected area; d) Schema of the MR structure; SEM images of (e) the cross section view of PS ridge waveguide and of (f) the two waveguides in the coupling region.

Following the fabrication steps, SEM measurements have been performed in order to verify the implementation of the PS MR. The cross section of the etched waveguide is reported in Fig. 1.e showing the PS core and cladding layers. A square core waveguide is obtained with

good etched edges with low roughness. The top view SEM image of the separation between the straight and the racetrack MR ridge waveguides, which appears in dark grey light (Fig. 1.f), shows that the gap has been successfully made along the coupling length of the racetrack.

2.3 Optical characterization setup

As shown in Fig. 2, the output from a tunable wavelength laser (Yenista Tunics T100S-HP), around 1550 nm, is coupled in the waveguide using a lensed fiber with a mode radius of 2 µm. A second lensed single mode fiber is also used to couple the output of the straight waveguide to a power-meter. Piezo-controlled stages are used to position the input and output fibers with the help of an infra-red camera. To make easier the analyses of the spectral responses of the MR, it is suitable to have one selected polarization to optimize the characteristics values, such as the quality factor Q and the contrast C, of the PS MR. Therefore, a polarization controller is placed between the laser and the input micro-lensed single mode fiber to select the TE mode which presents a better calculated sensitivity than TM one. A temperature controller is also used to maintain the sample at room temperature and to reduce the impact of temperature fluctuation on the spectral responses. The measurements of the spectral responses of the PS MR were done in the wavelength range of 1550-1554 nm with a step of 1 pm.

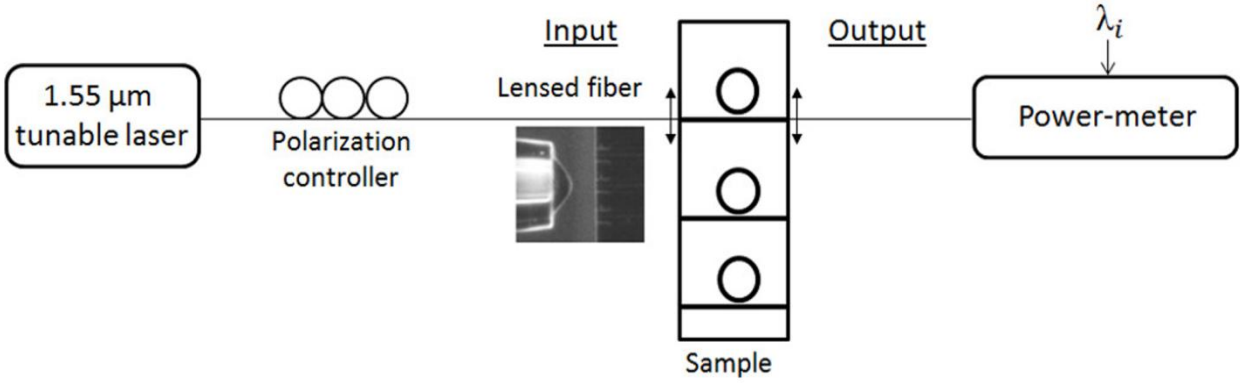

Fig. 2. Overview of the optical characterization setup.

3. Experimental

3.1. Optical characterizations

In order to calculate theoretical normalized transmission of the racetrack micro-resonator, the optical propagation losses have to be known. A cut-back method has been used to estimate the optical losses of the PS ridge waveguides. The transmitted power at the output of 5 PS waveguides of different lengths is measured and plotted in Fig. 3 as a function of the length L of the different waveguides.

The measurement uncertainties are attributed to the alignment of the micro-lensed fibers used to couple light into the waveguides and to the quality of the cleaved facet. The propagation, determined by the slope of a linear function, is estimated to 27 dB/cm at 1550 nm. This high value could be due to volume diffusion and principally to surface scattering and absorption of doped silicon [24]. This value is similar to reported propagation losses on PS ridge waveguide with an oxidation process at 500°C [19].

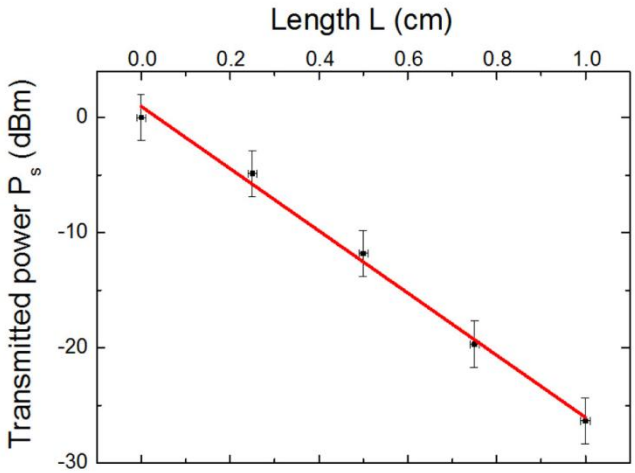

Fig. 3. Transmitted power as a function of the length variation of the PS ridge waveguides at 1550 nm.

Taken into account the experimental propagation losses, the theoretical spectral response of the PS micro-resonator is represented in Fig. 4.a for air superstrate. The theoretical quality factor of the PS MR is 7.10^3.

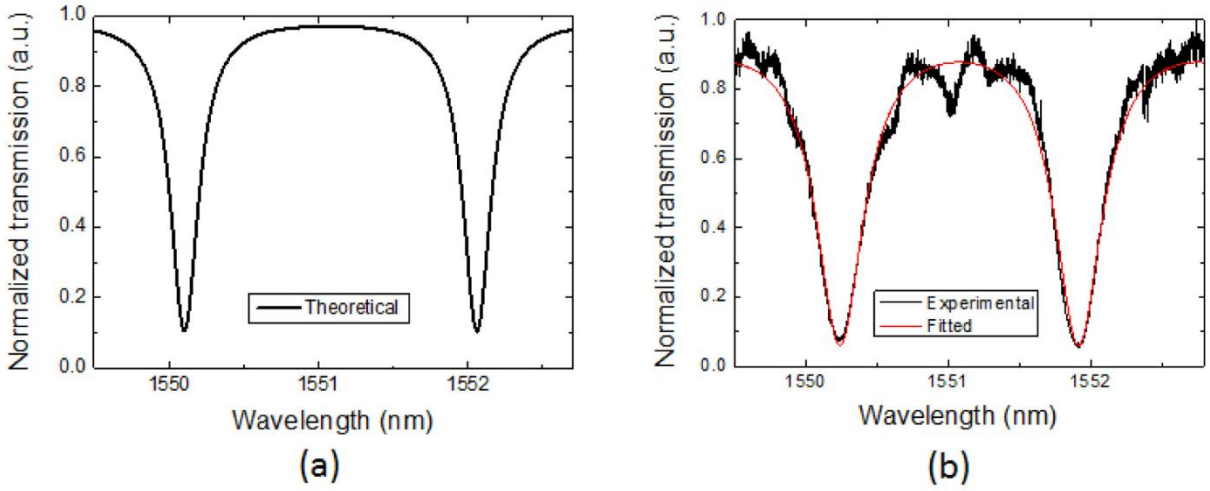

Fig. 4. (a) Theoretical transmission spectrum and (b) experimental and fitted transmission spectra. Both for TE polarization and air superstrate.

The experimental spectral response of the PS MR is measured with air superstrate. Then, calculated theoretical transmission is fitted to the experimental one to deduce the quality factor and optical losses and they are represented in Fig. 4.b. The quality factor of the PS MR, deduced from this theoretical transmission fit, is estimated to be 4.5 10^3. The difference between calculated and experimental quality factors can be explained by a difference between the theoretical propagation optical loss and the deduced one. Moreover, the difference could be also explained by a change of coupling ratio induced by the lower etched waveguide dimensions than the expected ones. Indeed, as reported in Fig. 1.e, a core height of 1.9 ± 0.1 µm and a width of 1.8 ± 0.1 µm are obtained experimentally. The top view SEM image of the separation between

the straight and the racetrack MR ridge waveguides, in Fig. 1.f, shows a gap of 0.7 µm ± 0.1 µm. This additional lateral etch leads to a different coupling ratio.

With regard to the detection application, the optical characterization of the PS MR with a water superstrate is performed. In the same way as with an air superstrate, firstly, a theoretical spectral response is calculated with the experimental propagation losses previously determined and shown in Fig. 5.a. The theoretical quality factor of the PS MR is $9.8.10^3$ for a water superstrate.

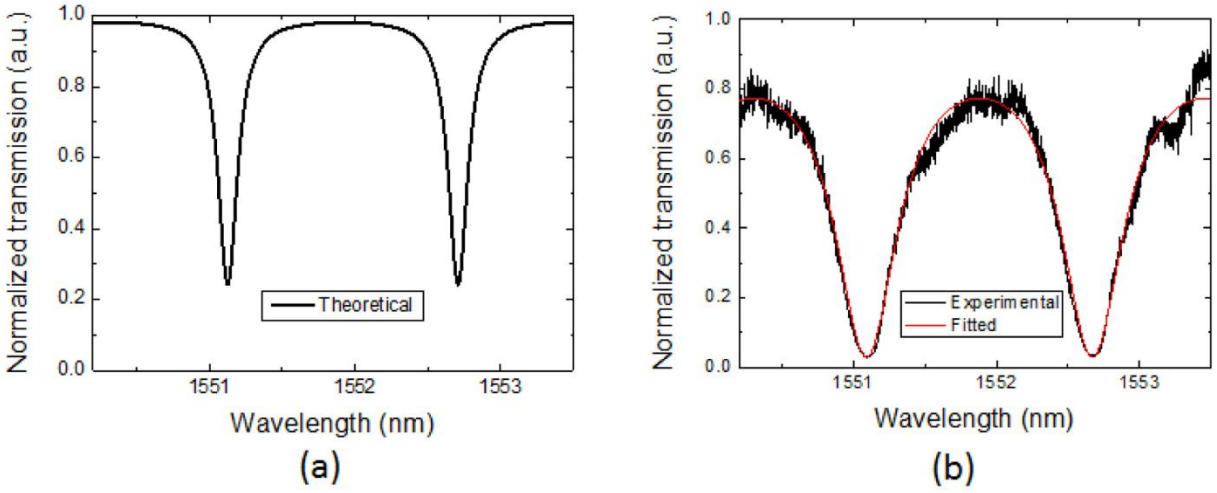

Fig. 5. (a) Theoretical transmission spectrum and (b) experimental and fitted transmission spectra. Both for TE polarization and water superstrate.

Calculated transmission spectra is fitted to an experimental one (Fig. 5.b) and from these spectra, a lower maximum transmission value and a lower quality factor of $3.6\ 10^3$, compared with the theoretical ones, are measured with aqueous environment. These differences are attributed to the high deduced optical losses of 68 dB/cm instead of the experimental ones of

27 dB/cm measured with air superstrate. So, the gap between the optical losses values could be mainly assigned to the high absorption coefficient of water equal to 9.6 cm^{-1} at 1550 nm [25] which corresponds to losses of 42 dB/cm.

3.2. Sensing application

As already mentioned before, PS MR is used as an optical transducer for glucose sensing applications. In order to evaluate the sensitivity of the structure by homogenous sensing, glucose aqueous solutions, with deionized water, were used with different concentrations from 0 to 15 g/L in order to obtain a wavelength shift lower than the free spectral range value. A micro-syringe is used to introduce the glucose solutions into the MR structure. The measurement of the transmission response is performed immediately after the placement of the drop on the MR. Between each measurement, the MR is rinsed with deionized water.

Glucose solution superstrate will induce a shift of the resonant wavelength towards higher wavelengths compared with the deionized water superstrate. To estimate the uncertainty on the resonant wavelength red-shift, the measurements are performed 3 times by removing the sample from the optical bench. The error on the red shift has been estimated to be 0.05 nm.

The refractive index of the glucose aqueous solution as a function of the concentration C of the solubilized glucose is given as [26]:

$$n_{glucose} = 1.189\ 10^{-4} \times C + n_{water} \qquad (1)$$

The experimental transmission spectra obtained with deionized water superstrate and with a glucosed aqueous solution using a concentration of 15 g/L are reported in Fig. 6. With this condition, the increase of refractive index is 1.8 10^{-3} and provides a resonant wavelength red-shift of 0.98 nm around 1550 nm.

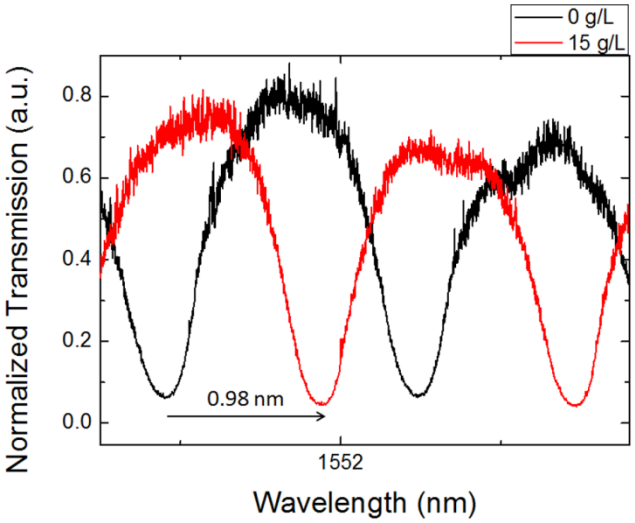

Fig. 6. Experimental transmission spectra, for TE polarization, with deionized water (0 g/L) and glucosed aqueous solution (15 g/L) superstrates on the PS MR.

In Fig. 7, the resonant wavelength red-shift $\Delta\lambda$ is plotted for the three different concentrations as a function of the refractive index variation of the glucose aqueous solution.

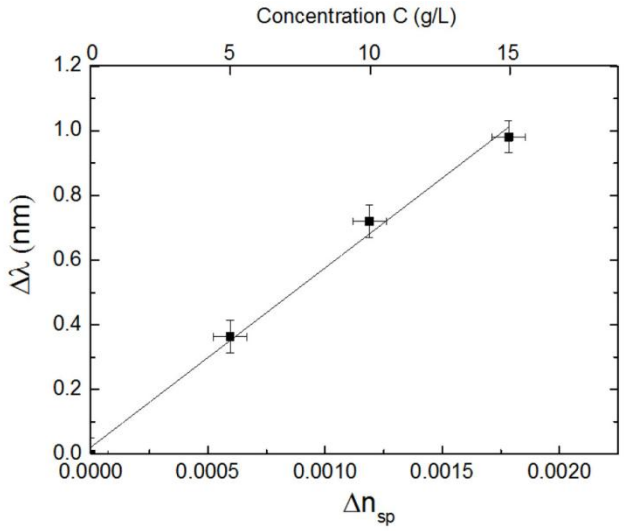

Fig. 7. Experimental transmission spectra, for TE polarization, with deionized water and glucose aqueous solution (15 g/L) superstrates on the PS MR.

The sensitivity of the PS MR is expressed by the ratio:

$$S = \frac{\Delta\lambda}{\Delta n_{sp}} \qquad (2)$$

and is determined by the slope of the linear fit. The experimental sensitivity S is then 559 ± 50 nm/RIU. The value obtained is higher than those currently presented in the literature for volume detection based on porous materials MR [19].

The limit of detection LOD, linked to the sensitivity and the quality factor, is expressed by [6]:

$$LOD = \frac{\delta\lambda}{10 \times S} \qquad (3)$$

with a δλ of 0.44 nm and the sensitivity S previously calculated, the PS MR sensor have a LOD of $(7.9 \pm 0.7).10^{-5}$ RIU which corresponds to a glucose concentration of (0.7 ± 0.1) g/L. This value is consistent with a diabetes application since the glucose concentration limit in the blood is 1.4 g/L [27].

4. Conclusion

This work presents the use of a PS racetrack MR as on optical transducer for sensing applications. The PS MR is based on ridge waveguides implemented by a standard photolithography process. In order to evaluate the sensitivity of the structure by homogenous sensing, glucose aqueous solutions were used with different concentrations. The characterization of the PS waveguides with an air superstrate shows propagation losses around 27 dB/cm. The PS racetrack MR shows a quality factor of $3.6\ 10^3$. We have measured a sensitivity of 559 ± 50 nm/RIU and a limit of detection of $(7.9 \pm 0.7).10^{-5}$ RIU, that is to our knowledge at the top of the state of art for one porous micro-resonator. To improve further the LOD of the sensor, the sensitivity could be increased further by the study of cascaded MR.

Acknowledgments

This work is funded by Département Côtes d'Armor (22), Région Bretagne and the CNRS. Technological processing of porous silicon ridges waveguides was performed on the CCLO clean room facilities of Foton. Financial support from University of Rennes 1 for HYPOP project and from CNRS for DETECT-COV project in the framework of the call "defi instrumentation aux limites 2017".

References

[1] V. Huet, A. Rasoloniaina, P. Guillemé, P. Rochard, P. Féron, M. Mortier, A. Levenson, K. Bencheikh, A. Yacomotti, Y. Dumeige, Physical Review Letters, **116** (2016) 133902.

[2] Y. Ruan, K. Boyd, H. Ji, A. François, H. Ebendorff-Heidepriem, J. Munch, T. M. Monro, Optics express, **22,** n°10 (2014) 11995 – 12006.

[3] S. Soria, S. Berneschi, M. Brenci, F. Cosi, G. Nunzi Conti, S. Pelli, and G. C. Righini, Sensors, **11** (2011) 785 – 805.

[4] F. Vollmer, S. Arnold, Nature Methods, **5**, n°7 (2008) 591 – 596.

[5] E. Kim, M. D. Baaske, F. Vollmer, Lab on a Chip, **17** (2017) 1190 – 1205.

[6] G. C. Righini, S. Soria, Sensors, **16**, n°6 (2016) 905 – 930.

[7] C.Y. Chao, W. Fung, L.J. Guo, Journal of lightwave technology, **24**, n°3 (2006) 1395 – 1402.

[8] G. D. Kim, G. S. Son, H. S. Lee, K. D. Kim, S. S. Lee, Optics Communications, **281** (2008) 4644 – 4647.

[9] C. Doolin, P. Doolin, B. C. Lewis, J. P. Davis, Applied Physics Letters, **106** (2014) 081104-1 – 081104-4.

[10] T. Hutter, N. Bamiedakis, S. R. Elliott, Proceeedings of COMSOL Conference, Paris (2010).

[11] S. M. Weiss, G. Rong, JL. Lawrie, Physica E **41** (2009) 1071 – 1075.

[12] Y. Zhao, G. A. Rodriguez, Y. M. Graham, T. Cao, G. Gaur, S. M. Weiss, Proc. SPIE, **10081** (2017) 100810D.

[13] P. Steiner, F. Kozlowski, W. Lang, Applied Physics Letters, **62** (1993) 2700 – 2702.

[14] A. Foucaran, F. Pascal-Delannoy, A. Giani, A. Sackda, P. Combete, A. Boyer, Thin Film Solid **297** (1996) 317 – 320.

[15] F. A. Harraz, Sensors and Actuators B: Chemical **202** (2014) 897 – 912.

[16] S. Chan, P. M. Fauchet, Y. Li, L. J. Roberg, B. L. Miller, Phys. Status Solidi A, **182** (2000) 541 – 546.

[17] S. Dhanekar, S. Jain, Biosensors and bioelectronics **41** (2013) 54 – 64.

[18] G. Rong, A. Najmaie, J. E. Sipe, S. M. Weiss, Biosensors and Bioelectronics, **23** (2008) 1572-1576.

[19] G. A. Rodriguez, H. Shuren, S. M. Weiss, Optics Express **23**, n° 6 (2015) 7111 – 7119.

[20] J. E. Lugo, J. A. Del Rio, J. J. Tagüeña-Martínez, Journal of Applied Physics, **81** (1997) 1923 – 1928.

[21] N. Lorrain, M. Hiraoui, M. Guendouz, L. Haji, Material Science and Engineering B **176** (2011) 1047 – 1053.

[22] E. V. Astrova, V. A. Tolmachev, Materials Science and Engineering B **69** (2000) 142-148.

[23] P. Girault, N. Lorrain, J. Lemaitre, L. Poffo, M. Guendouz, I. Hardy, M. Gadonna, A. Gutierrez, L. Bodiou, J. Charrier, Optical Materials **50** (2015) 167 – 174.

[24] P. Pirastesh, J. Charrier, Y. Dumeige, S. Haesaert, P. Joubert, Journal of Applied Physics **101** (2007) 083110-1 – 083110-6.

[25] W. M. Irvine, J. B. Pollack, Icarus, **8** (1968) 324-360.

[26] C. Ciminelli, F. Dell'Olio, D. Conteduca, C. M. Campanella, M. N. Armenise, Optics and Laser Technology, **59** (2014) 60-67.

[27] S. Liakat, K. A. Bors, L. Xu, C. M. Woods, J. Doyle, C. F. Gmachl, Optics Express, **5**, n°7 (2015) 7111-7119.